Urban Classification Using Full Spectral Information of Landsat ETM+ Imagery in Marion County, Indiana

Dengsheng Lu and Qihao Weng

Abstract

This paper compares different image processing routines to identify suitable remote sensing variables for urban classification in the Marion County, Indiana, USA, using a Landsat 7 Enhanced Thematic Mapper Plus (ETM+) image. The ETM+ multispectral, panchromatic, and thermal images are used. Incorporation of spectral signature, texture, and surface temperature is examined, as well as data fusion techniques for combining a higher spatial resolution image with lower spatial resolution multispectral images. Results indicate that incorporation of texture from lower spatial resolution images or of a temperature image cannot improve classification accuracies. However, incorporation of textures derived from a higher spatial resolution panchromatic image improves the classification accuracy. In particular, use of data fusion result and texture image yields the best classification accuracy with an overall accuracy of 78 percent and a kappa index of 0.73 for eleven land use and land cover classes.

Introduction

Accurate image classification results are a prerequisite for many environmental and socioeconomic applications (Jensen and Cowen, 1999), such as urban change detection (Ward *et al.*, 2000), urban heat islands (Lo *et al.*, 1997; Weng, 2001), and estimation of biophysical, demographic, and socioeconomic variables (Lo, 1995; Thomson and Hardin, 2000). However, generating a satisfactory classification image from remotely sensed data is not a straightforward task. Many factors contribute to this difficulty, including (a) the characteristics of a study area, (b) availability of suitable remotely sensed data, ancillary and ground reference data, (c) proper use of variables and classification algorithms, (d) the analyst's experience, and (e) the time constraint. Urban landscapes are typically composed of features that are smaller than the spatial resolution of the sensors: a complex combination of buildings, roads, grass, trees, soil, and water (Jensen, 2000). This characteristic of urban landscapes makes mixed pixels a common problem in medium spatial resolution data (between 10 to 100 m spatial resolutions) such as Landsat TM/ETM+. Such a mixture becomes especially prevalent in residential areas where buildings, trees, lawns, concrete, and asphalt can all occur within a pixel. The low accuracy of land cover classification in urban areas is largely attributed to the mixed pixel problem.

As fine spatial resolution data (better than 5 m spatial resolution), such as Ikonos (Sugumaran *et al.*, 2002; van der Sande *et al.*, 2003) and ADAR digital multispectral scanner imagery (Thomas *et al.*, 2003), become easily available in recent years, they have been increasingly utilized for urban studies. A major advantage of these fine spatial resolution imageries is that such data greatly reduce the mixed pixel problem, providing the potential to extract much more detailed information of urban structures compared with medium spatial resolution data. However, a new severe problem comes with the fine spatial resolution image data, i.e., the shade problem caused by topography, tall buildings, or trees (Asner and Warner, 2003). Moreover, high spectral variation within any land-cover class often decreases the classification accuracy. The huge amount of data storage and severe shade problem in fine spatial resolution image give rise to challenges for selection of suitable image processing approaches and classification algorithms over a large area. Last but not least, high spatial resolution imagery is much more expensive and requires much more time to implement data analysis than medium spatial resolution image data.

In practice, medium spatial resolution imagery, especially the TM/ETM+ being readily available for multiple dates, is still the most commonly used data for urban classification, in spite of the mixed pixel problem. Different approaches have been used in order to improve urban classification accuracy. These approaches can be roughly grouped into four categories: (a) use of sub-pixel information (Rashed *et al.*, 2001; Phinn *et al.*, 2002), (b) data integration of different sensors or sources (Harris and Ventura, 1995; Haack *et al.*, 2002), (c) making full use of the spectral information of a single sensor (Gong and Howarth, 1992; Stuckens *et al.*, 2000; Shaban and Dikshit, 2001), and (d) use of expert knowledge (Stefanov *et al.*, 2001; Hung and Ridd, 2002). Traditional per-pixel classification algorithms, such as maximum likelihood classifier (MLC), are still frequently used for image classification due to their simplicity and availability. However, much attention has been shifted to develop more advanced techniques and classification algorithms, such as neural network, contextual, object oriented, and knowledge-based classification approaches in

Dengsheng Lu is with the Center for the Study of Institutions, Population, and Environmental Change, Indiana University, Bloomington, Indiana 47408 (dlu@indiana.edu).

Qihao Weng is with the Department of Geography, Geology, and Anthropology, Indiana State University, Terre Haute, Indiana 47809 (geweng@isugw.indstate.edu).

Photogrammetric Engineering & Remote Sensing
Vol. 71, No. 11, November 2005, pp. 1275–1284.

0099-1112/05/7111–1275/$3.00/0

the past decade (Stuckens *et al.*, 2000; Zhang and Foody, 2001; Thomas *et al.*, 2003; Zhang and Wang, 2003).

Making full use of remote sensing information may be the most efficient and effective way to improve classification accuracy. Remote sensing data has spectral, spatial, temporal, polarization, and other characteristics. One of the critical steps is to select suitable remote-sensing variables for classification. Much previous research used SPOT HRV data for urban classification due to its high spatial resolution comparing with Landsat TM data (Franklin and Peddle, 1990; Marceau *et al.*, 1990; Gong *et al.*, 1992; Shaban and Dikshit, 2002). High spatial resolution is considered to be more important than high spectral resolution in urban classification (Jensen and Cowen, 1999). The enhanced characteristic of ETM+ data, compared with TM, adds a panchromatic band of 15 m spatial resolution, and also increases the spatial resolution of thermal infrared (TIR) band to 60 m. Figure 1 illustrates some typical urban features in different spatial resolution images; in the aerial photograph of 5 m spatial resolution, buildings and roads can be easily observed, but in the panchromatic image with 15 m spatial resolution, the shapes of buildings and some narrow roads in residential areas disappeared. As spatial resolution deceased to 30 m in the ETM+ band 5 and 60 m in the TIR image, interpretation of buildings became nearly impossible. Urban remote sensing has used the ETM+ multispectral bands, but has not fully utilized the panchromatic and TIR bands for urban classification. The panchromatic image with 15 m spatial resolution not only reduces mixed pixels, but also provides a rich texture and contextual information than multispectral bands with 30 m spatial resolution. Use of surface temperatures derived from the TIR band may also be helpful for urban classification owing to its unique spectral characteristic. Therefore, it may be assumed that incorporation of higher spatial resolution panchromatic band or addition of temperature image into multispectral images improves urban classification performance.

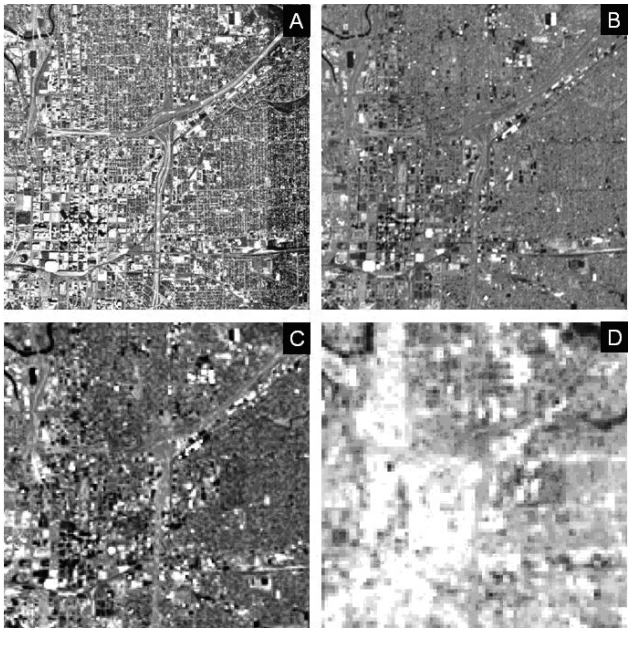

Figure 1. Impact of spatial resolution on image interpretation. (a) aerial photograph with 5 m spatial resolution, (b) ETM+ Panchromatic image with 15 m spatial resolution, (c) ETM+ short-wave infrared image (band 5) with 30 m spatial resolution, and (d) temperature image from ETM+ thermal band with 60 m spatial resolution.

This paper will examine the potential roles of high spatial resolution panchromatic band and relatively low spatial resolution TIR band in improving urban classification accuracy, and attempt to identify a suitable remote sensing procedure(s) for urban classification through a comparative study of different image processing routines. To be specific, this paper will examine the use of textures from multispectral bands and from the panchromatic band, surface temperatures, data fusion technique, and the combination of data fusion and texture for improving urban classification accuracies.

Background

Use of Texture Information

Many texture measures have been developed (Haralick *et al.*, 1973; Kashyap *et al.*, 1982; Emerson *et al.*, 1999), and used for land cover classification (Marceau *et al.*, 1990; Augusteijn *et al.*, 1995; Groom *et al.*, 1996; Podest and Saatchi, 2002; Chen *et al.*, 2004). Franklin and Peddle (1990) indicated that use of textures from grey level co-occurrence matrix (GLCM) and spectral features of SPOT HRV data improved overall classification accuracy. Gong *et al.* (1992) compared GLCM, simple statistical transformations (SST), and texture spectrum (TS) approaches with SPOT HRV data, and found that certain textures derived from GLCM and SST could improve urban classification accuracy. Shaban and Dikshit (2001) investigated GLCM, grey level difference histogram (GLDH), and sum and difference histogram (SADH) textures from SPOT spectral data in an Indian urban environment, and found that a combination of texture and spectral features significantly improved the classification performance. Compared with the result using pure spectral features, approximately 9 percent and 17 percent improvement were achieved for an addition of one and two textures, respectively. They further found that contrast, entropy, variance, and inverse difference moment provided higher accuracy than other tested texture measures and the best sizes of moving window were 7×7 and 9×9. Use of multiple or multi-scale texture images should be in conjunction with spectral information to improve classification results (Kurosu *et al.*, 2001; Shaban abd Dikshit, 2001; Butusov, 2003). However, for a specific study, there are not straightforward ways for identifying suitable texture measures because texture varies with the characteristics of the landscape under investigation and image data used. Identifying suitable textures involve determination of texture measure, image band, and the size of the moving window (Franklin *et al.*, 1996; Chen *et al.*, 2004).

Data Fusion

Image data from different sensors have their own strengths and limitations. The techniques of data fusion or integration of multi-sensor or multi-resolution data take advantage of the strengths of distinct data for improvement of visual interpretation and quantitative analysis. In general, three levels of data fusion can be identified (Gong, 1994), i.e., pixel, feature, and decision. Data fusion involves two steps of merging procedures: geometrical co-registration of two datasets and mixture of spectral and spatial information contents to generate a new dataset that contains the improved information from both datasets. Accurate registration between the two datasets is extremely significant for precisely extracting the information contents from both datasets, especially when line features such as roads and rivers are the objects of concern.

Many methods have been developed to blend spectral and spatial information. Solberg *et al.* (1996) divided the methods of data fusion into four categories: statistical, fuzzy logic, Dempster-Shafer evidence theory, and neural network. Dai and Khorram (1998) presented a hierarchical data fusion system for vegetation classification. Pohl and Van Genderen (1998) reviewed methods for fusion of multi-sensor data, including color related techniques (e.g., color composite, intensity-hue-saturation (IHS) and luminance-chrominance, statistical/numerical methods (e.g., arithmetic combination, principal component analysis (PCA), high pass filtering, regression variable substitution, canonical variable substitution, component substitution, and wavelets), and various combinations of the above methods. Among these methods, IHS transformation was identified to be the most frequently used method for improving visual display of multi-sensor data (Welch and Ehlers, 1987), but the IHS approach can only employ three bands and the resultant image may be not suitable for further quantitative analysis such as classification. PCA is often used for data fusion because it can produce an output result that better preserves the spectral integrity of the input dataset. In recent years, wavelet-merging techniques have shown to be another effective approach to generate a better improvement of spectral and spatial information contents (Li *et al.*, 2002; Simone *et al.*, 2002; Ulfarsson *et al.*, 2003). Previous research has suggested that integration of multi-sensor or multi-resolution data, such as TM and radar (Ban, 2003; Haack *et al.*, 2002), SPOT HRV and TM (Welch and Ehlers, 1987; Yocky, 1996), and SPOT multispectral and panchromatic bands (Garguet-Duport *et al.*, 1996; Shaban and Dikshit, 2002), would improve classification results.

Data Transformation

It is well known that remotely sensed data are highly correlated between the adjacent spectral bands, such as the visible bands in Landsat TM/ETM+ (Barnsley, 1999). Image transformation techniques are often used to reduce the number of image channels, so that the information contents would be concentrated on a few transformed bands (Jensen, 1996). Several techniques have been developed to transform the data from highly correlated bands into an orthogonal dataset. The PCA, tasseled cap, and minimum noise fraction, are among the most commonly used methods (Oetter *et al.*, 2000; Wu and Linders, 2000). These methods have some common characteristics: (a) these transforms are linear combinations of the original spectral bands; (b) these transforms project the original data into a new coordinate set; and (c) the majority of information is concentrated on limited principal components (PC) which are uncorrelated or weakly correlated with each other. In practice, PCA is the most frequently used approach in many applications, such as used for reduction of data dimension, data fusion, and change detection. PCA is used in this research for reduction of data dimension and for data fusion of higher spatial resolution panchromatic band with lower spatial resolution multispectral bands.

Study Area

The City of Indianapolis within Marion County, Indiana, United States, was chosen as the study area (Figure 2). Indianapolis, the state capital, is a key center for manufacturing, warehousing, distribution, and transportation in the state. With almost 800,000 population, the city is the nation's twelfth largest. It possesses several other advantages that make it an appropriate choice for such a study. It has a single central city and other large urban areas in which the vicinity has not influenced its growth. The city is located in a flat plain, and is relatively symmetrical, having possibilities of expansion in all directions. Like most American cities, Indianapolis is increasing in population and in area. The areal expansion is through encroachment into the adjacent agricultural and non-urban land. Certain decision-making factors such as density of population, distance to work, property value, and income structure encourage some sectors of the metropolitan Indianapolis to expand faster than others. Accurate classification of urban land-use and land-cover (LULC) types is significant to understand, to control, and to plan its future development.

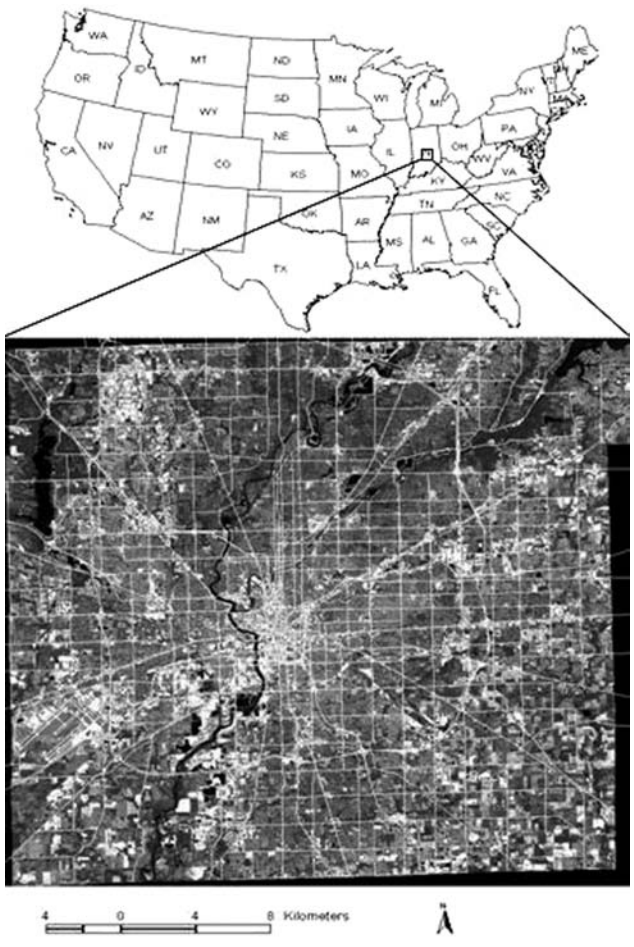

Figure 2. The study area: Marion County, Indiana, USA (Road layer overlaid on ETM+ band 7 image).

Methods

Image Preprocessing

A Landsat 7 ETM+ image (path 21/row 32) of Marion County, Indiana, which was acquired on 22 June 2000, was used in this study. The data was radiometrically converted to at-sensor reflectance using an image-based correction method (Markham and Barker, 1987). The image was rectified to a common Universal Transverse Mercator coordinate system based on 1:24 000 scale topographic maps, and was resampled to a pixel size of 30 m by 30 m using the nearest neighbor resampling algorithm. The root mean square error of less than 0.5 pixels was achieved during the rectification.

Color orthophotographs, which were dated March and April of 2002, were used as ground reference data for collection of training and test sample plots. The orthophotographs have a spatial resolution of 0.5 foot (i.e., 0.14 m). The coordinate system is Indiana State Plane East, Zone 1301 in NAD83. Nine orthophotographs covering the whole study area were obtained and registered to the same projection as the ETM+ image and re-sampled to 5 m pixel size for quicker display and reduced computing time. The orthophotographs were then mosaiced into one image of the study area.

Texture Analysis

Incorporation of texture and spectral information has been proved to be effective in improving classification accuracy (Shaban and Dikshit, 2001; Butusov, 2003). Following research conducted by Shaban and Dikshit (2001), variance associated with a window size of 9 × 9 was selected as a texture measure and used in this study. In order to examine the significance of textures in improving classification performance, variance textures were calculated for the multispectral bands 3, 4, and 5 with 30 m spatial resolution and for the panchromatic band with 15 m spatial resolution. The variance is mathematically expressed as

$$Var = \frac{\sum_{i,j=0}^{n-1}(X_{ij} - \frac{1}{n}\sum_{i,j=0}^{n-1} X_{ij})^2}{n-1} \quad (1)$$

where X_{ij} is the reflectance value of pixel (i, j), and n is the number of pixels in a window. Figure 3 provides a part of the study area for a comparison of textures from ETM+ bands 3, 4, 5, and panchromatic band. Textures from ETM+ bands 3, 4, and 5 seem over-smoothed and lost much detailed information, but the texutre from panchromatic band appeared a better visual interpretation effect than those from lower spatial resolution multispectral bands.

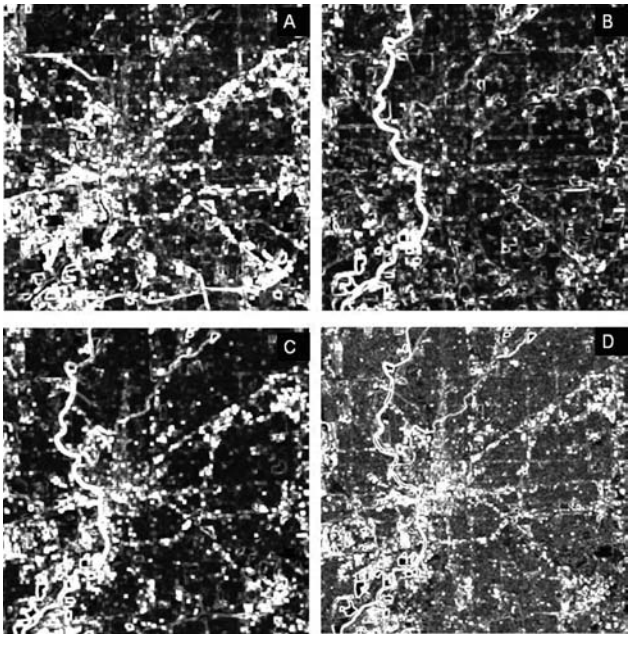

Figure 3. Texture images derived from the variance texture measure associated with different bands and spatial resolution images. (a) texture based on ETM+ band 3 with 30 m spatial resolution, (b) texture based on ETM+ band 4 with 30 m spatial resolution, (c) texture based on ETM+ band 5 with 30 m spatial resolution, and (d) texture based on ETM+ panchromatic band with 15 m spatial resolution.

Surface Temperature Computation

The thermal infrared (TIR) image was converted to a surface temperature map according to the following procedure (Weng *et al.*, 2004). The digital number (DN) of Landsat ETM+ TIR band was first converted into spectral radiance using Equation 2, and then converted to at-satellite brightness temperature (i.e., blackbody temperature, T_B) under the assumption of uniform emissivity using Equation 3 (Landsat Project Science Office, 2002):

$$L_\lambda = 0.0370588 \times \text{DN} + 3.2, \quad (2)$$

$$T_B = \frac{K_2}{\ln\left(\frac{K_1}{L_\lambda} + 1\right)}. \quad (3)$$

where T_B is effective at-satellite temperature in Kelvin, L_λ is spectral radiance in watts/(meters squared × ster × μm); and K_2 and K_1 are pre-launch calibration constants. For Landsat-7 ETM+, K_2 = 1282.71 K and K_1 = 666.09 mWcm^{-2} sr$^{-1}\mu$m^{-1} were used.

The emissivity corrected land surface temperatures (T_s) were finally computed as follows (Artis and Carnhan, 1982):

$$T_S = \frac{T_B}{1 + (\lambda \times T_B/\rho)\ln\varepsilon}, \quad (4)$$

where: λ is the wavelength of emitted radiance [for which the peak response and the average of the limiting wavelengths (λ = 11.5 μm) (Markham and Barker, 1985) were used], $\rho = h \times c/\sigma$ (1.438 × 10^{-2} mK), σ = Stefan Bolzmann's constant (5.67 × 10^{-8} W m^{-2} K^{-4} = 1.38 × 10^{-23} J/K), h = Planck's constant (6.626 × 10^{-34} J sec), c = velocity of light (2.998 × 10^8 m/sec), and ε is spectral emissivity.

Principal Component Analysis

PCA was used for two purposes in this research: reducing data dimension and implementing data fusion. Due to high correlation between bands (note: the correlation coefficients are 0.985 and 0.970 between bands 1 and 2 and between bands 2 and 3, respectively), data redundancy was significant in the ETM+ data. PCA projected the original dataset into a new coordinate set with no correlation between the new images. The first principal component (PC1) was a sum of different bands, highlighting the overall brightness. The PC2 was a difference between the sum of bands 4 and 5 and the sum of visible bands and band 7, enhancing vegetation information; and PC3 the difference between short-wave infrared bands (TM 5 and TM 7) and the sum of visible bands and near infrared band (Table 1). The PC1 contained the largest percentage of the data variance and the second PC the second largest data variance, and so on (Table 1). The higher components appeared noisy because they contained very little variance, much of which was due to noise in the original spectral data. In this study, the first three components accounted for 99.28 percent of total variance.

The data fusion procedure based on the PCA approach integrated the ETM+ multispectral and the panchromatic images according to the following steps: (a) transforming ETM+ multispectral bands into six PCs, (b) re-mapping the panchromatic image into the data range of PC1, (c) substituting the PC1 with the panchromatic image, and (d) applying an inverse PCA to the data. One crucial step when using this

TABLE 1. EIGENVECTOR AND EIGENVALUE FROM PRINCIPAL COMPONENT ANALYSIS

	ETM+ Bands						Eigenvalue and Percentage		
PC	Band 1	Band 2	Band 3	Band 4	Band 5	Band 7	Eig_val.	%	Accu%
PC1	0.418	0.399	0.472	0.208	0.482	0.410	4227.45	78.21	78.21
PC2	−0.102	−0.136	−0.358	0.854	0.305	−0.144	915.40	16.94	95.15
PC3	−0.506	−0.313	−0.138	−0.299	0.577	0.452	223.43	4.13	99.28
PC4	−0.551	−0.047	0.547	0.358	−0.424	0.295	18.71	0.35	99.63
PC5	−0.344	0.165	0.424	−0.099	0.396	−0.713	16.38	0.30	99.93
PC6	0.369	−0.834	0.389	0.033	0.067	−0.107	3.8	0.07	100

approach is to perform a histogram matching between the histogram of a panchromatic image and that of the PC1.

Figure 4 compares the results of PCA and data fusion with the original Landsat image data. It indicates that PC1 highlighted the impervious surfaces of the study area. The panchromatic image provided more detailed information due to its higher spatial resolution. Comparing the data fusion result with the original ETM+ band 5, the new image clearly enhanced spatial details, especially linear features.

Image Classification

To identify the most suitable method(s) for improving urban classification accuracy, different image processing routines were designed (Table 2). The following questions were examined in the process of image classification: (a) would the use of the first three PCs from PCA of the ETM+ multispectral bands increase or decrease classification accuracy? (b) would incorporation of textures from 30 m multispectral bands improve classification accuracy? (c) would incorporation of a texture from 15 m panchromatic band improve classification accuracy? (d) would incorporation of surface temperature improve classification accuracy? (e) would incorporation of both texture and surface temperature improve classification accuracy? (f) would a data fusion of panchromatic and multispectral images improve classification accuracy? and (g) would incorporation of data fusion and texture images improve classification accuracy?

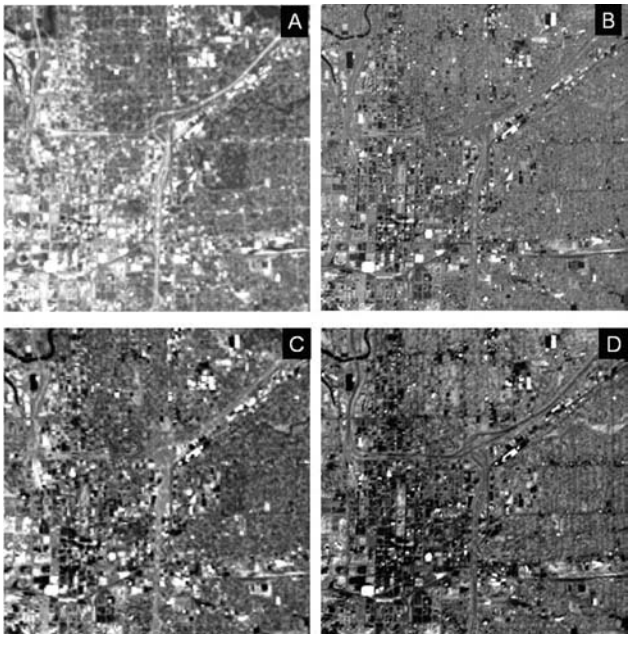

Figure 4. A comparison of the urban landscapes before and after image transformations. (a) the first component from PCA (30 m spatial resolution), (b) panchromatic image (15 m spatial resolution), (c) original ETM+ band 5 image (30 m spatial resolution), and (d) band 5 image after data fusion using PCA (15 m spatial resolution).

Before implementing image classification, the selection of a suitable classification scheme is important. By visually analyzing the ETM+ color composite and comparing with the orthophotography images, a total of seventeen land-use and land-cover (LULC) classes were identified. Because of the complexity of urban landscapes, the same LULC classes may have different spectral characteristics. Initial LULC classes included two urban types (large buildings with very high reflectance and buildings with relative lower reflectance), three types of transportation (wide highways, narrow highway, and roads), high density residential, low density residential, non-vegetation wetland, three types of crops, fallow, grass, pasture, upland forest, wetland forest, and water. Figure 5 gives a comparison among commercial, high-density, and low-density residential lands.

After initial image interpretation, two classification schemes with six- and eleven-classes were finally selected (Table 3). In the classification scheme with eleven classes, two building types and three transportations were merged into the commercial/industrial/transportation lands (CIT), and three types of crops combined as one. In the classification scheme with six classes, cropland, fallow, and pastures were further grouped as agricultural land, while upland forest and wetland forest combined into the forest class. High-density and low-density residential lands were merged to create a residential class.

Training sample plots were selected from the 2002 color orthophotography. Fifteen to twenty sample plots were selected for each class. The spectral response curves of selected sample plots for each class were analyzed to ensure that they have similar reflectance characteristics within the class, but have distinct response patterns between the classes. Next, the transformed divergence index was computed to analyze the separability of the selected classes. After refining the training sample data, the maximum likelihood classification (MLC) algorithm was applied to classify the images. The resultant thematic images were merged into eleven and six classes, respectively, and a majority filter with 3×3 window size was applied to remove the noise in the classified images.

Accuracy Assessment

Accuracy assessment is considered an important step in evaluation of different image processing routines in image classification (Foody, 2002). The meaning and calculation for overall accuracy, producer's accuracy, user's accuracy, and kappa coefficient have been described extensively in the literature (Congalton, 1991; Janssen and van der Wel, 1994; Smits *et al.*, 1999; Foody, 2002). An error matrix was constructed to assess the result of each classification, with which

TABLE 2. IMAGE CLASSIFICATION METHODS INVESTIGATED

No.	Code	Method
1*	ETM	ETM+ multispectral image (excluding thermal and panchromatic bands)
2*	PCA	The first three components derived from PCA of ETM+ multispectral image
3*	B345Text	Combination of spectral bands (ETM+ multispectral bands) and textural data (three textures based on variance associated with 9 × 9 window size and ETM+ bands 3, 4, and 5.
4	Pantext	Combination of spectral bands (ETM+ multispectral bands) and textural data (variance associated with 9 × 9 window size and panchromatic image)
5*	Temp	Combination of spectral bands (ETM+ multispectral bands) and temperature (derived from TIR band)
6	Pantext-Temp	Combination of spectral bands (ETM+ multispectral bands), textural data (variance associated with 9 × 9 window size and panchromatic image), and temperature (derived from TIR band)
7	Pan-Fusion	Data fusion using PCA method based on ETM+ multispectral bands and one panchromatic band
8	Fusion-Pantext	Combination of data fusion image (using PCA method) and texture (derived from panchromatic image using variance associated with 9 × 9 window size)

Note: *1, 2, 3, and 5 approaches used 30 m spatial resolution images, others used 15 m spatial resolution images because they used panchromatic bands with 15 m spatial resolution.

pertinent accuracy assessment parameters can be derived. A total of 350 test samples were randomly selected and examined using color orthophotography for accuracy assessment. The overall accuracy, producer's accuracy, user's accuracy, and kappa coefficient were calculated for each classified image.

Results

Table 4 provides a comparison of accuracy assessment results among different image processing routines using the classification scheme II, and Table 5 provides a comparison based on the classification scheme I. Because of similar nature between the two tables, the following analysis focuses on the classification scheme II.

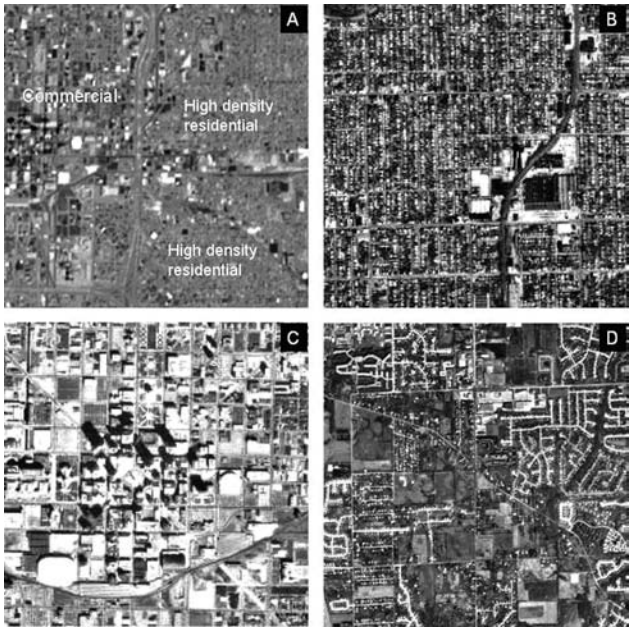

Figure 5. Examples of commercial, high-density and low- density residential lands. (a) panchromatic image illustrating commercial and high density residential lands, (b) aerial photograph illustrating high density residential lands, (c) aerial photograph illustrating commercial lands, and (d) aerial photograph illustrating low density residential lands.

In the classification result with the ETM+ multispectral data (Method 1), an overall accuracy of 70.6 percent was achieved. CIT, LDR, FAL, PAS, and WAT have higher accuracies (greater than 79 percent of PA and 72 percent of UA) than other classes. The main confusion come from the following pairs of LULC classes: (1) CIT and HDR; (2) CRP, PAS, and GRA; (3) UPF and WLF; and (4) UPF and LDR. The following compares other processing methods with Method 1, so as to determine whether an image processing method will improve the classification accuracy.

The overall classification accuracy of Method 2, which used the first three components of the ETM+ multispectral data, is 68.3 percent, a similar level of accuracy to Method 1. Compared to Method 1, the accuracies of LDR, CRP, and FAL classes were decreased, but the performance of WLF and PAS classes were improved. CIT, HDR, and GRA remained the same level of accuracies. The confusions between CRP and GRA, between UPF and LDR, and between WLF and UPF continued to affect the classification performance. In addition, the fourth PC had revealed some useful information for classification of CRP and UPF, but contained dominantly noise. Method 2 could be very useful for image classification of a large area, since it could greatly reduce image storage and classification time.

Method 3 has a poorer performance than Method 1, with an overall classification accuracy of 62.3 percent. Method 3 combined the multispectral image with three textures that were developed from ETM+ bands 3, 4, and 5 associated with a 9 × 9 window size. The classification accuracies of almost all classes were reduced marginally. This implies that selected textures had smoothed the differences among the LULC classes, especially between the HDR and LDR, between UPF and WLF, and between CRP and GRA (see Figure 3). In contrast, Method 4 clearly outperforms Method 1. The overall accuracy of 74 percent was achieved, an improvement of 3.4 percent. The combination of multispectral data with a texture image derived from the panchromatic band improved the classification accuracies of most LULC classes. Confusions between CRP and GRA and between UPF and WLF were substantially minimized. It is apparent that textures derived from higher spatial resolution data could provide much more useful information than those derived from lower spatial resolution data (Figure 3).

Incorporation of a temperature image in the classification did not improve the classification result. Method 5

TABLE 3. DEFINITION OF LAND-USE AND LAND-COVER CLASSIFICATION SCHEMES

Classification Scheme I	Code I	Classification Scheme II	Code II	Definition
Commercial/industrial/ transportation lands	CIT	Commercial/industrial/ transportation lands	CIT	Highly developed areas, mainly for commercial or industrial use, including transportation
Residential	RES	High density residential	HDR	Highly developed areas where people reside in high numbers
		Low density residential	LDR	A mixture of constructed materials and vegetation, population density is lower than in high density residential areas
Forest	FOR	Upland forest	UPF	Areas dominated by dense vegetations
		Wetland forest	WLF	Areas covered by forest but the soil is periodically saturated with water
Agricultural lands	AGR	Crops	CRP	Different crops in agricultural lands
		Fallow	FAL	Areas used for the production of crops that are temporarily barren or with sparse vegetation cover.
		Non-vegetation wetland	NVW	Areas where the soil is periodically saturated with water
		Pastures	PAS	Areas of grasses used for livestock grazing or the production of hay crops
Grass	GRA	Grass	GRA	Vegetation planted in developed settings for recreation
Water	WAT	Water	WAT	All areas of open water

TABLE 4. ACCURACY ASSESSMENT OF DIFFERENT IMAGE CLASSIFICATION METHODS WITH ELEVEN LAND-USE AND LAND-COVER CLASSES

	Method 1		Method 2		Method 3		Method 4		Method 5		Method 6		Method 7		Method 8	
	ETM		PCA		B345Text		Pantext		Temp		Pantext-Temp		Pan-Fusion		Fusion-Pantext	
LULC types	PA%	UA%	PA%	UA%	PA%	UA%	PA%	UA%	PA%	UA%	PA%	UA%	PA%	UA%	PA%	UA%
CIT	79.41	85.71	79.41	85.71	95.59	61.90	86.76	84.29	75.00	77.27	92.65	76.83	71.64	96.00	88.24	93.75
HDR	82.35	41.18	82.35	41.18	35.29	60.00	70.59	70.59	64.71	57.89	52.94	60.00	83.33	41.67	70.59	66.67
LDR	82.35	72.41	78.43	70.80	63.73	75.58	90.20	66.67	80.39	67.21	85.29	69.60	79.41	69.83	94.12	68.09
UPF	66.67	90.91	66.67	86.96	50.00	88.24	66.67	100.00	50.00	88.24	73.33	100.00	70.00	91.30	76.67	92.00
WLF	33.33	30.00	55.56	50.00	22.22	40.00	55.56	35.71	44.44	50.00	55.56	62.50	77.78	41.18	100.00	69.23
CRP	69.23	58.70	58.97	47.92	33.33	59.09	51.28	95.24	58.97	82.14	51.28	86.96	66.67	57.78	51.28	86.96
FAL	81.82	90.00	72.73	80.00	81.82	75.00	72.73	80.00	81.82	90.00	81.82	81.82	81.82	100.00	81.82	100.00
NVW	75.00	50.00	75.00	42.86	50.00	66.67	50.00	50.00	75.00	60.00	50.00	50.00	75.00	60.00	50.00	50.00
PAS	100.00	75.00	100.00	100.00	100.00	75.00	100.00	75.00	100.00	75.00	100.00	75.00	100.00	100.00	100.00	75.00
GRA	34.55	67.86	34.55	65.52	49.09	40.30	47.27	72.22	56.36	50.82	47.27	57.78	41.82	71.88	49.09	75.00
WAT	91.67	100.00	83.33	100.00	91.67	57.89	100.00	75.00	83.33	100.00	91.67	100.00	100.00	85.71	100.00	92.31
OCA	70.57		68.29		62.29		74.00		69.14		73.43		70.86		78.00	
OKS	0.6446		0.6176		0.5423		0.6800		0.6218		0.6730		0.6501		0.7290	

Note: PA – Producer's Accuracy; UA – User's Accuracy; OCA – Overall Classification Accuracy; OKS – Overall Kappa Statistics

TABLE 5. ACCURACY ASSESSMENT OF DIFFERENT IMAGE CLASSIFICATION METHODS WITH SIX LAND-USE AND LAND-COVER CLASSES

	Method 1		Method 2		Method 3		Method 4		Method 5		Method 6		Method 7		Method 8	
	ETM		PCA		B345Text		Pantext		Temp		Pantext-Temp		Pan-Fusion		Fusion-Pantext	
LULC types	PA%	UA%	PA%	UA%	PA%	UA%	PA%	UA%	PA%	UA%	PA%	UA%	PA%	UA%	PA%	UA%
CIT	76.47	85.25	76.47	89.66	94.12	59.26	85.29	84.06	70.59	78.69	92.65	75.00	70.59	100.00	88.24	93.75
RES	91.60	71.24	88.24	70.00	67.23	85.11	92.44	70.97	87.39	72.22	89.08	76.26	91.60	71.71	98.32	73.13
AGR	80.70	68.66	78.95	64.29	56.14	76.19	64.91	94.87	71.93	85.42	64.91	90.24	80.70	71.88	63.16	90.00
GRA	36.36	71.43	34.55	65.52	49.09	40.91	47.27	68.42	52.73	47.54	45.45	55.56	40.00	70.97	49.09	79.41
FOR	66.67	83.87	66.67	78.79	48.72	86.36	76.92	90.91	53.85	87.50	74.36	96.67	84.62	80.49	89.74	89.74
WAT	83.33	100.00	83.33	100.00	83.33	55.56	100.00	75.00	83.33	83.33	91.67	100.00	100.00	85.71	100.00	92.31
OCA	75.14		73.43		66.29		78.00		72.29		77.43		77.14		82.00	
OKS	0.6742		0.6527		0.5737		0.712		0.639		0.7063		0.7022		0.7636	

Note: PA – Producer's Accuracy; UA – User's Accuracy; OCA – Overall Classification Accuracy; OKS – Overall Kappa Statistics

produces an overall accuracy of 69.1 percent. Some classes, such as CIT, HDR, LDR, and UPF decreased in accuracy, although the accuracy of other classes, such as WLF, did rise. The slight difference of thermal response pattern among the classes, such as LDR and UPF, did not help separating them. Furthermore, the low spatial resolution of the Landsat ETM+ TIR band (60 m, as compared with 30 m for the multispectral bands) may smooth the inherent differences between certain

classes (see Figure 1). Method 6 is similar to Method 5, but added a texture image derived from the panchromatic band for classification. A global classification accuracy of 73.4 percent was achieved. Clearly, this improvement is attributable to the texture image from the panchromatic band, not to the temperature image. The most significant improvement lies in the distinction between UPF and WLF.

Methods 7 and 8 employed the technique of data fusion. The former merged the ETM+ multispectral and the panchromatic bands using the PCA fusion method, and the latter combined the data fusion image (resulted from Method 7) with a texture image derived from the panchromatic band. Method 7 did not significantly improve the overall accuracy, but the classification accuracy of certain classes improved, including UPF, WLF, FAL, and GRA. In contrast, the classification accuracy of LDR declined slightly. The confusion between LDR and UPF remained as spatial resolution increased. This implies that although data fusion with different spatial resolution images is becoming as a popular approach for image classification, the increased spectral variation within a class may degrade the distinction among certain classes, and thus the overall classification accuracy. This is especially true for LDR due to its complex composition of the materials and increased spectral variation within the LDR class. Method 8 has the best performance among all the methods examined. Almost all selected classes augmented their classification accuracies to a certain degree. In particular, the confusion between CIT and HDR reduced, so did between LDR and UPF. It is concluded that the combination of data fusion and texture is an effective way to improve LULC classification accuracy. The data fusion of the panchromatic and multispectral bands restrained the mixed pixel problem, while the texture image from the panchromatic band moderated the problem of spectral variation within a class.

Discussion and Conclusions

Image classification in urban landscapes using medium spatial resolution data is a challenging task. Major confusion exists among GRA, PAS, and CRP, between UPF and LDR, and between CIT and HDR. Texture and temperature may improve classification accuracy for some classes, but may degrade other classes. Data fusion using multispectral and high spatial resolution panchromatic images are useful for improving classification accuracy, but high spatial resolution also increases spectral variation within the classes, decreasing classification accuracy. Incorporation of data fusion and texture information derived from high spatial resolution image can significantly improve the classification accuracy. This study demonstrates that incorporation of texture information from the Landsat ETM+ panchromatic image improved the overall accuracy by 3.4 percent, while use of data fusion and the texture improved by 7.4 percent, compared to the use of pure multispectral signatures of the ETM+ image.

Incorporation of texture and spectral signatures is conventionally assumed to provide better classification results than use of pure spectral signatures (Shaban and Dikshit, 2001; Butusov, 2003). However, the success for incorporating texture images depends on the type of texture measure, image used to derive textures, and the selection of moving window size. For example, this study found that incorporation of variance texture associated with window size of 9 by 9 and image bands 3, 4, and 5 degraded the classification accuracy, whereas incorporation of the same texture measure but using the panchromatic image of 15 m spatial resolution improved the classification accuracy. Caution needs to be taken when texture measures are used to extract specific information in different study areas because textures depend on the characteristics of a study area and the image data used. The increase of spatial resolution results in an increasing importance of texture in image classification. For medium spatial resolution data, large moving window sizes may smooth the differences among the land cover classes, leading to lower classification accuracy. As spatial resolution increases, it is necessary to determine a sufficiently large moving window size(s), because a small size(s) of window would enhance the noise.

Differences in thermal response among different land cover types may be used to improve classification results. However, this study indicates that incorporation of a temperature image did not improve the overall classification accuracy. Some classes generated even lower accuracy. This can be attributed to the low spatial resolution of the thermal band in the ETM+ sensor. Slight differences of temperatures among land cover types contributed little in improving classification at a local scale. However, similar types of temperature information may be helpful for regional or national land cover classification.

Image transform is often used in image processing to reduce the dimension of image data and to condense the information contents onto a limited number of components. This is especially useful for hyperspectral data because of high correlation and large data redundancy. Although the majority of information contents are concentrated in the first three components, use of other components may be necessary. For example, this study indicates that the fourth component contains some information on crops and forests, and the fifth component contains information about roads. Due to a large amount of noise in these components, it is necessary to remove them before use.

Data fusion of multi-sensor or multi-resolution data is often used to enhance visual interpretation and quantitative analysis to extract information contents from different data sources. Selection of a data fusion method for use depends on the study objectives and the algorithm available. This study indicates that data fusion using the PCA approach can improve classification accuracy of certain classes. Incorporation of Landsat ETM+ panchromatic band with the multispectral data reduced the number of mixed pixels, resulting in improvement of classification accuracy. However, higher spatial resolution data also possess high spectral variations within the same land cover, leading to lower classification accuracy. This study proves that a combination of data fusion image and texture produced a better classification result than other classification methods, due to the fact that texture can reduce the variation within the land cover classes.

Due to the complexity of urban landscapes and the limitations of current sensor technology, the methodology used in this study, i.e., the combination of data fusion and texture measures can successfully improve image classification only to a certain degree. Confusion among land cover types still exists. Recently, sub-pixel analysis using spectral mixture models, which un-mix an image into different fractions, has also demonstrated effective for improving classification accuracy (Rashed *et al.*, 2001; Phinn *et al.*, 2002; Lu and Weng, 2004). Spectral unmixing provides a more realistic representation of the true nature of a surface compared with that provided by the assignment of a single dominant class to every pixel by statistical models (Campbell, 2002), and is suitable to solve the mixture problem for medium or low spatial resolution data. Further studies are warranted by incorporation of fraction images, texture, or other variables/data for image classification. Moreover, commonly used parametric classifiers, i.e., MLC, may not be very suitable for urban classification, since the histogram of the features of interest is often not normally distri-

buted. Use of nonparametric classifiers should be advocated, including neural network, decision tree, and other suitable classifiers. It is certain that future research would hold great promise in the areas of data fusion, spectral mixture analysis, and texture measurement in conjunction with the use of advanced nonparametric classifiers.

Acknowledgments

The authors acknowledge the financial support of University Research Committee at Indiana State University through the Grant No.UNR184 and from the Center for the Study of Institutions, Population, and Environmental Change (CIPEC), Indiana University, through the National Science Foundation (Grant 99-06826). The authors also wish to thank three anonymous reviewers for their constructive comments and suggestions.

References

Artis, D.A., and W.H. Carnahan, 1982. Survey of emissivity variability in thermography of urban areas, *Remote Sensing of Environment*, 12:313–329.

Asner, G.P., and A.S. Warner, 2003. Canopy shadow in IKONOS satellite observations of tropical forests and savannas, *Remote Sensing of Environment*, 87:521–533.

Augusteijn, M.F., L.E. Clemens, and K.A. Shaw, 1995. Performance evaluation of texture measures for ground cover identification in satellite images by means of a neural network classifier, *IEEE Transactions on Geoscience and Remote Sensing*, 33:616–625.

Ban, Y., 2003. Synergy of multitemporal ERS-1 SAR and Landsat TM data for classification of agricultural crops, *Canadian Journal of Remote Sensing*, 29:518–526.

Barnsley, M.J., 1999. Digital remote sensing data and their characteristics, *Geographical Information Systems: Principles, Techniques, Applications, and Management*, Second Edition (P. Longley, M. Goodchild, D.J. Maguire, and D.W. Rhind, editors), John Wiley and Sons, New York, New York, pp. 451–466.

Butusov, O.B., 2003. Textural classification of forest types from Landsat 7 imagery, *Mapping Sciences and Remote Sensing*, 40:91–104.

Campbell, J.B., 2002. *Introduction to Remote Sensing*, Third Edition, The Guilford Press, New York, New York, 621 p.

Chen, D., D.A. Stow, and P. Gong, 2004. Examining the effect of spatial resolution and texture window size on classification accuracy: an urban environment case, *International Journal of Remote Sensing*, 25:2177–2192.

Congalton, R.G., 1991. A review of assessing the accuracy of classification of remotely sensed data, *Remote Sensing of Environment*, 37:35–46.

Dai, X., and S. Khorram, 1998. A hierarchical methodology framework for multisource data fusion in vegetation classification, *International Journal of Remote Sensing*, 19:3697–3701.

Emerson, C.W., N.S. Lam, and D.A. Quattrochi, 1999. Multi-scale fractal analysis of image texture and pattern, *Photogrammetric Engineering & Remote Sensing*, 65:51–61.

Foody, G.M., 2002. Status of land cover classification accuracy assessment, *Remote Sensing of Environment*, 80:185–201.

Franklin, S.E., and D.R. Peddle, 1990. Classification of SPOT HRV imagery and texture features, *International Journal of Remote Sensing*, 11:551–556.

Franklin, S.E., M.A. Wulder, and M.B. Lavigne, 1996. Automated derivation of geographic window sizes for remote sensing digital image texture analysis, *Computers and Geosciences*, 22:665–673.

Garguet-Duport, B., J. Girel, J. Chassery, and G. Pautou, 1996. The use of multiresolution analysis and wavelet transform for merging SPOT panchromatic and multispectral image data, *Photogrammetric Engineering & Remote Sensing*, 62:1057–1066.

Gong, P., 1994. Integrated analysis of spatial data from multiple sources: an overview, *Canadian Journal of Remote Sensing*, 20:349–359.

Gong, P., and P.J. Howarth, 1992. Frequency-based contextual classification and gray-level vector reduction for land-use identification, *Photogrammetric Engineering & Remote Sensing*, 58:423–437.

Gong, P., D.J. Marceau, and P.J. Howarth, 1992. A comparison of spatial feature extraction algorithms for land-use classification with SPOT HRV data, *Remote Sensing of Environment*, 40:137–151.

Groom, G.B., R.M. Fuller, and A.R. Jones, 1996. Contextual correction: techniques for improving land cover mapping from remotely sensed images, *International Journal of Remote Sensing*, 17:69–89.

Haack, B.N., E.K. Solomon, M.A. Bechdol, and N.D. Herold, 2002. Radar and optical data comparison/integration for urban delineation: a case study, *Photogrammetric Engineering & Remote Sensing*, 68:1289–1296.

Haralick, R.M., K. Shanmugam, and I. Dinstein, 1973. Textural features for image classification, *IEEE Transactions on Systems, Man and Cybernetics*, SMC-3:610–620.

Harris, P.M., and S.J. Ventura, 1995. The integration of geographic data with remotely sensed imagery to improve classification in an urban area, *Photogrammetric Engineering & Remote Sensing*, 61:993–998.

Hung, M, and M.K. Ridd, 2002. A subpixel classifier for urban land-cover mapping based on a maximum-likelihood approach and expert system rules, *Photogrammetric Engineering & Remote Sensing*, 68:1173–1180.

Janssen, L.F.J., and F.J.M. van der Wel, 1994. Accuracy assessment of satellite derived land-cover data: a review, *Photogrammetric Engineering & Remote Sensing*, 60:419–426.

Jensen, J.R., 1996. *Introductory Digital Image Processing: A Remote Sensing Perspective* Second Edition, Prentice Hall, Upper Saddle River, New Jersey, 318 p.

Jensen, J.R., 2000. *Remote Sensing of the Environment: An Earth Resource Perspective*, Prentice Hall, Upper Saddle River, New Jersey, 544 p.

Jensen, J.R., and D.C. Cowen, 1999. Remote sensing of urban/suburban infrastructure and socioeconomic attributes, *Photogrammetric Engineering & Remote Sensing*, 65:611–622.

Kashyap, R.L., R. Chellappa, and A. Khotanzad, 1982. Texture classification using features derived from random field models, *Pattern Recognition Letters*, 1:43–50.

Kurosu, T., S. Yokoyama, and K. Chiba, 2001. Land use classification with textural analysis and the aggregation technique using multi-temporal JERS-1 L-band SAR images, *International Journal of Remote Sensing*, 22:595–613.

Landsat Project Science Office, 2002. *Landsat 7 Science Data User's Handbook*, Goddard Space Flight Center, NASA, Washington, D.C. URL: http://ltpwww.gsfc.nasa.gov/IAS/handbook/handbook_toc.html (last date accessed: 02 August 2005).

Li, S., J.T. Kwok, and Y. Wang, 2002. Using the discrete wavelet frame transform to merge Landsat TM and SPOT panchromatic images, *Information Fusion*, 3:17–23.

Lo, C.P., 1995. Automated population and dwelling unit estimation from high-resolution satellite images: a GIS approach, *International Journal of Remote Sensing*, 16:17–34.

Lo, C.P., D. Quattrochi, and J. Luvall, 1997. Application of high-resolution thermal infrared remote sensing and GIS to assess the urban heat island effect, *International Journal of Remote Sensing*, 18:287–304.

Lu. D., and Q. Weng, 2004. Spectral mixture analysis of the urban landscapes in Indianapolis with Landsat ETM+ imagery, *Photogrammetric Engineering & Remote Sensing*, 70:1053–1062.

Marceau, D.J., P.J. Howarth, J.M. Dubois, and D.J. Gratton, 1990. Evaluation of the grey-level co-occurrence matrix method for land-cover classification using SPOT imagery, *IEEE Transactions on Geoscience and Remote Sensing*, 28:513–519.

Markham, B.L., and J. Barker, 1985. Spectral characteristics of the LANDSAT Thematic Mapper sensors, *International Journal of Remote Sensing*, 6:697–716.

Markham, B.L., and J. Barker, 1987. Thematic Mapper bandpass solar exoatmospheric irradiances, *International Journal of Remote Sensing*, 8:517–523.

Oetter, D.R., W.B. Cohen, M. Berterretche, T.K. Maiersperger, and R.E. Kennedy, 2000. Land cover mapping in an agricultural setting using multiseasonal Thematic Mapper data, *Remote Sensing of Environment*, 76:139–155.

Phinn, S., M. Stanford, P. Scarth, A.T. Murray, and P.T. Shyy, 2002. Monitoring the composition of urban environments based on the vegetation-impervious surface-soil (VIS) model by subpixel analysis techniques, *International Journal of Remote Sensing*, 23:4131–4153.

Pohl, C., and J.L. van Genderen, 1998. Multisensor image fusion in remote sensing: concepts, methods, and applications, *International Journal of Remote Sensing*, 19:823–854.

Podest, E., and S. Saatchi, 2002. Application of multiscale texture in classifying JERS-1 radar data over tropical vegetation, *International Journal of Remote Sensing*, 23:1487–1506.

Rashed, T., J.R. Weeks, M.S. Gadalla, and A.G. Hill, 2001. Revealing the anatomy of cities through spectral mixture analysis of multisepctral satellite imagery: a case study of the Greater Cairo region, Egypt, *Geocarto International*, 16:5–15.

Shaban, M.A., and O. Dikshit, 2001. Improvement of classification in urban areas by the use of textural features: the case study of Lucknow city, Uttar Pradesh, *International Journal of Remote Sensing*, 22:565–593.

Shaban, M.A., and O. Dikshit, 2002. Evaluation of the merging of SPOT multispectral and panchromatic data for classification of an urban environment, *International Journal of Remote Sensing*, 23:249–262.

Simone, G., A. Farina, F.C. Morabito, S.B. Serpico, and L. Bruzzone, 2002. Image fusion techniques for remote sensing applications, *Information Fusion*, 3:3–15.

Smits, P.C., S.G. Dellepiane, and R.A. Schowengerdt, 1999. Quality assessment of image classification algorithms for land-cover mapping: a review and a proposal for a cost-based approach, *International Journal of Remote Sensing*, 20:1461–1486.

Solberg, A.H.S., T. Taxt, and A.K. Jain, 1996. A Markov random field model for classification of multisource satellite imagery, *IEEE Transactions on Geoscience and Remote Sensing*, 34:100–112.

Stefanov, W.L., M.S. Ramsey, and P.R. Christensen, 2001. Monitoring urban land cover change: an expert system approach to land cover classification of semiarid to arid urban centers, *Remote Sensing of Environment*, 77:173–185.

Stuckens, J., P.R. Coppin, and M.E. Bauer, 2000. Integrating contextual information with per-pixel classification for improved land cover classification, *Remote Sensing of Environment*, 71:282–296.

Sugumaran, R., D. Zerr, and T. Prato, 2002. Improved urban land cover mapping using multitemporal Ikonos images for local government planning, *Canadian Journal of Remote Sensing*, 28:90–95.

Thomas, N., C. Hendrix, and R.G. Congalton, 2003. A comparison of urban mapping methods using high-resolution digital imagery, *Photogrammetric Engineering & Remote Sensing*, 69:963–972.

Thomson, C.N., and P. Hardin, 2000. Remote sensing/GIS integration to identify potential low-income housing sites, *Cities*, 17:97–109.

Ulfarsson, M.O., J.A. Benediktsson, and J.R. Sveinsson, 2003. Data fusion and feature extraction in the wavelet domain, *International Journal of Remote Sensing*, 24:3933–3945.

van der Sande, C.J., S.M. de Jong, and A.P.J. de Roo, 2003. A segmentation and classification approach of IKONOS-2 imagery for land cover mapping to assist flood risk and flood damage assessment, *International Journal of Applied Earth Observation and Geoinformation*, 4:217–229.

Ward, D., S.R. Phinn, and A.L. Murray, 2000. Monitoring growth in rapidly urbanizing areas using remotely sensed data, *Professional Geographer*, 53:371–386.

Welch, R., and M. Ehlers, 1987. Merging multi-resolution SPOT HRV and Landsat TM data, *Photogrammetric Engineering & Remote Sensing*, 53:301–303.

Weng, Q., 2001. A remote sensing-GIS evaluation of urban expansion and its impact on surface temperature in the Zhujiang Delta, China, *International Journal of Remote Sensing*, 22:1999–2014.

Weng, Q., D. Lu, and J. Schubring, 2004. Estimation of land surface temperature-vegetation abundance relationship for urban heat island studies, *Remote Sensing of Environment*, 89:467–483.

Wu, D., and J. Linders, 2000. Comparison of three different methods to select features for discriminating forest cover types using SAR imagery, *International Journal of Remote Sensing*, 21:2089–2099.

Yocky, D.A., 1996. Multiresolution wavelet decomposition image merger of Landsat Thmatic Mapper and SPOT panchromatic data, *Photogrammetric Engineering & Remote Sensing*, 62:1067–1074.

Zhang, J., and G.M. Foody, 2001. Fully-fuzzy supervised classification of sub-urban land cover from remotely sensed imagery: statistical neural network approaches, *International Journal of Remote Sensing*, 22:615–628.

Zhang, Q., and J. Wang, 2003. A rule-based urban land use inferring method for fine-resolution multispectral imagery, *Canadian Journal of Remote Sensing*, 29:1–13.

(Received 04 June 2004; accepted 29 September 2004; revised 19 October 2004)